Inorganic Chemistry

pubs.acs.org/IC

Forum Article

# Thermal Treatment Effect on CO and NO Adsorption on Fe(II) and Fe(III) Species in $Fe_3O$-Based MIL-Type Metal−Organic Frameworks: A Density Functional Theory Study

Jenny G. Vitillo* and Laura Gagliardi*

Cite This: *Inorg. Chem.* 2021, 60, 11813−11824

Read Online

ACCESS | Metrics & More | Article Recommendations | Supporting Information

**ABSTRACT:** The properties of metal−organic frameworks (MOFs) based on triiron oxo-centered ($Fe_3O$) metal nodes are often related to the efficiency of the removal of the solvent molecules and the counteranion chemisorbed on the $Fe_3O$ unit by postsynthetic thermal treatment. Temperature, time, and the reaction environment play a significant role in modifying key features of the materials, that is, the number of open metal sites and the reduction of Fe(III) centers to Fe(II). IR spectroscopy allows the inspection of these postsynthetic modifications by using carbon monoxide (CO) and nitric oxide (NO) as probe molecules. However, the reference data sets are based on spectra recorded for iron zeolites and oxides, whose structures are different from the $Fe_3O$ one. We used density functional theory to study how the adsorption enthalpy and the vibrational bands of CO and NO are modified upon dehydration and reduction of $Fe_3O$ metal nodes. We obtained a set of theoretical spectra that can model the modification observed in previously reported experimental spectra. Several CO and NO bands were previously assigned to heterogeneous Fe(II) and Fe(III) sites, suggesting a large defectivity of the materials. On the basis of the calculations, we propose an alternative assignment of these bands by considering only crystallographic iron sites. These findings affect the common description of $Fe_3O$-based MOFs as highly defective materials. We expect these results to be of interest to the large community of scientists working on Fe(II)- and Fe(III)-based MOFs and related materials.

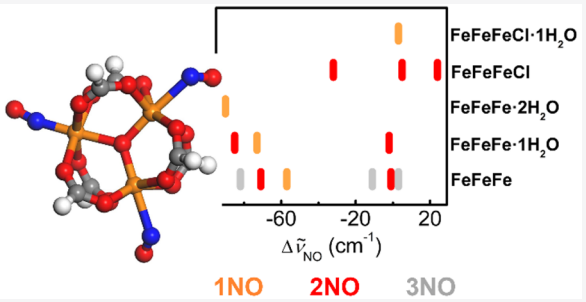


## 1. INTRODUCTION

Metal−organic frameworks (MOFs) based on a triiron oxo-centered cluster ($Fe_3O$)[1,2] are important materials for several applications, including gas storage and separation,[3−5] heat pump applications,[6,7] catalysis,[8−10] and drug delivery.[1,11,12] The most representative of this class of MOFs are MIL-100(Fe)[2] and MIL-101(Fe) (MIL = Materials Institute Lavoisier).[13] In the as-synthesized material, the metal node has the formula $[Fe^{III}_3(\mu_3\text{-}O)(X)(Z)_2]^{6+}$ (Figure 1a), where Z is a solvent molecule (e.g., water) and X is a counteranion.[5] The anion originates from the reagents used in the MOF synthesis (e.g., −OH from NaOH or KOH, −F from HF, and −Cl from iron chloride salts). More than one kind of X and Z can be present in the same material.

Upon heating of the material in a vacuum or in a flow of inert gas, both the X and Z species can be removed from the metal node, creating an open iron site that can coordinate an adsorbate.[5] The oxidation state of the iron centers does not change upon the removal of Z. The removal of X, instead, causes the reduction of one Fe(III) to Fe(II). This means that upon increasing the temperature we can go from the as-synthesized sample, having all of the nodes with the formula $[Fe^{III}_3(\mu_3\text{-}O)(X)(Z)_2]^{6+}$ (Figure 1a), to a fully activated MOF with $[Fe^{II}Fe^{III}_2(\mu_3\text{-}O)]^{6+}$ metal nodes (Figure 1b). At intermediate temperatures, clusters with different compositions coexist, having the general formula $[Fe^{II}_xFe^{III}_y(\mu_3\text{-}O)(X)_l(Z)_n]^{6+}$, with $x = 0$ and 1, $y = 3 - x$, $l = 1 - x$; $0 \le n \le 2 + x$. The presence of open iron centers and, in particular Fe(II) sites, has been considered to be one of the reasons for the successful performance of $Fe_3O$-based MOFs in catalysis[8,9] and gas separation.[3−5] It is then important to evaluate the efficacy of the possible postsynthetic protocols in order to tailor the number of open Fe(II) and Fe(III) species for the different purposes. Vibrational and Mössbauer spectroscopies[4,5,9,14] and microcalorimetry[4] are commonly used to optimize postsynthetic protocols involving the iron centers as the thermal treatment of these materials and the grafting of guest species.[15] IR spectroscopy using nitric oxide (NO) and carbon monoxide (CO) as molecular probes is particularly suitable for the characterization of iron-based materials because the stretching frequency of these molecules is shifted to different spectral regions if they are coordinated to Fe(II) or Fe(III) centers.[16,17]

**Special Issue:** Postsynthetic Modification of Metal-Organic Frameworks

**Received:** April 5, 2021
**Published:** June 10, 2021

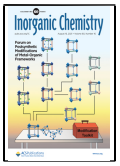

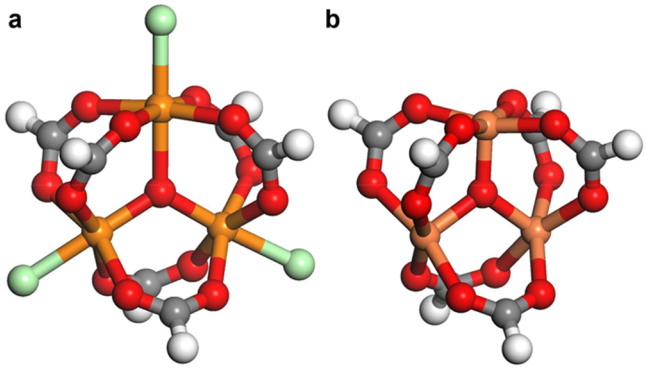


**Figure 1.** Models of the triiron oxo-centered metal clusters formed upon thermal treatment in MIL-100(Fe) at different temperatures (all lower than the decomposition temperature of the MOF): (a) $[Fe^{III}_3(\mu_3\text{-}O)(X)(H_2O)_2](HCOO)_6$ ($Fe_3O$-X·$2H_2O$) as a model of the as-synthesized material; (b) $[Fe^{II}Fe^{III}_2(\mu_3\text{-}O)](HCOO)_6$ ($Fe_3O$) model of the fully activated material, where the counterion (X) and all of the water molecules have been removed. Structures are optimized at the UM06-L/def2-TZVP level. All of the other clusters can be obtained from part a by the removal of X and/or water. Color code: green, water or X; red, oxygen; gray, carbon; orange, iron; white, hydrogen.

IR spectroscopy of CO and NO is an efficient diagnostic tool to determine the iron oxidation state in MOF materials. Previous spectroscopic studies on MIL-100(Fe) suggested the presence of heterogeneous Fe(II) and Fe(III) sites.[5,14] Nevertheless, no explanation of the origin of this heterogeneity was provided besides its possible correlation with the presence of an unreacted linker[18] in the material and the presence of defects.[5] In fact, the only data that can be used for the assignment of the NO and CO bands in IR spectra in Fe-based MOFs are based on studies on oxides and zeolites,[5,14] whose structures are different compared to that of the $Fe_3O$ cluster. The study of CO and NO adsorption on $Fe_3O$-based MOFs is relevant to gas separation and therapeutics. NO removal from exhaust gases is an important process.[19] CO removal from $H_2$ and $CH_4$ is a mandatory step for their safe use in fuel cells.[4,20] NO[21−23] and CO[22] are also important gasotransmitters in physiological and biological functions. MIL-100(Fe) and MIL-101(Fe) are among the most studied MOFs for drug delivery because of their high capacity and low toxicity.[1,11,12] Understanding how the presence of water modifies the interaction of NO and CO with the drug carrier is pivotal for these applications because water triggers the gas release.[4] Moreover, the effect of water on NO and CO adsorption in MOFs is important because water is often present as a contaminant in many gas mixtures and can affect the separations.

In this study, we used Kohn−Sham density functional theory (DFT) methods to determine if the presence of water molecules and of X influences the adsorption enthalpy and stretching frequency of CO and NO in $Fe_3O$-based materials. The effect of CO and NO coverage was also evaluated. We considered two X, −OH and −Cl, to assess the vibrational shift of the molecular probes. We adopted cluster models, namely, $[Fe^{II}_xFe^{III}_y(\mu_3\text{-}O)(X)_l(Z)_n]^{6+}$ units coordinated to six formates. Seven different models were considered: $[Fe^{II}Fe^{III}_2(\mu_3\text{-}O)](HCOO)_6$ ($Fe_3O$ in the following; see Figure 1b), $[Fe^{II}Fe^{III}_2(\mu_3\text{-}O)(H_2O)](HCOO)_6$ ($Fe_3O{\cdot}1H_2O$), $[Fe^{II}Fe^{III}_2(\mu_3\text{-}O)(H_2O)_2](HCOO)_6$ ($Fe_3O{\cdot}2H_2O$), $[Fe^{III}_3(\mu_3\text{-}O)Cl](HCOO)_6$ ($Fe_3O$-Cl), $[Fe^{III}_3(\mu_3\text{-}O)(OH)](HCOO)_6$ ($Fe_3O$-OH), $[Fe^{III}_3(\mu_3\text{-}O)Cl(H_2O)](HCOO)_6$ ($Fe_3O$-Cl·$1H_2O$), and $[Fe^{III}_3(\mu_3\text{-}O)(OH)(H_2O)](HCOO)_6$ ($Fe_3O$-OH·$1H_2O$). On the basis of our results, we propose an alternative assignment to the one generally accepted in the literature of the IR bands of CO[4,5,14] and NO[14,24] adsorbed in $Fe_3O$-based MOFs by considering only crystallographic sites.

## 2. COMPUTATIONAL METHODS

DFT calculations were performed using the M06-L functional[25] in its unrestricted formalism (U) in combination with the def2-TZVP basis sets,[26,27] as implemented in the *Gaussian 16* program.[28] Previous investigations showed that this level of theory correctly reproduces the electronic properties of iron centers in MOFs,[29] in particular $Fe_3O$, when benchmarked versus multireference calculations.[8] The $Fe_3O$ model has been previously employed to describe $N_2O$ reactivity on MIL-100.[9] Moreover, this model has been used by Mavrandonakis et al.[30] to predict the adsorption enthalpies and vibrational frequencies of different adsorbates in trimetal oxo-centered MOFs. This model has shown results similar to those reported for a cluster coordinated to benzoate instead of formate groups in reactivity[31] and in adsorption studies.[30]

Geometry optimizations were carried out by means of the Berny optimization algorithm with an analytical gradient. A (99, 590) pruned grid was used (i.e., 99 radial points and 590 angular points per radial point). The *Gaussian 16* default convergence thresholds were set for optimization. All of the energetic data were corrected for basis set superposition error (BSSE) following the a posteriori method proposed by Boys and Bernardi,[32] as implemented in *Gaussian 16*. The energy and enthalpy of adsorption for the complex with $(n+1)$ L molecules are defined as

$$\Delta Y_L = Y_{(n+1)L/cluster} - Y_{nL/cluster} - Y_L$$

The BSSE-corrected values, indicated by a c superscript, were obtained from the computed $Y$ values as

$$Y^c = Y + \mathrm{BSSE}$$

Unscaled harmonic frequencies were obtained analytically. Enthalpies and Gibbs free energies were calculated at 1 atm and 298 K using the scheme proposed by De Moor et al.,[33] whereby low-lying frequency modes (<50 $cm^{-1}$) were replaced by a cutoff value (50 $cm^{-1}$) in the calculation of the vibrational partition functions.[34−38] Charge and spin densities were obtained using Charge Model 5 (CM5)[39] and Hirshfeld population analysis,[40] respectively. Spin densities are expressed as the difference between the $\alpha$ and $\beta$ electron densities.

## 3. RESULTS AND DISCUSSION

The dependence on the temperature of the water and X [or Fe(II)] content in $Fe_3O$-based MOFs was determined experimentally in previous studies.[4,5] We summarize prior results to guide the reader in a comparison between our computational results and the experimental ones. Leclerc et al.[5] treated MIL-100(Fe) (X = 81% F, OH, trimesate) in a dynamic vacuum in the 25−300 °C range: they observed the complete removal of free and bonded water at 150 °C, with the formation of only a small fraction of Fe(II). Above 150 °C, the concentration of Fe(II) increases with the temperature: Yoon et al.[4] reported a maximal removal of 40% of the initial Fe−X sites at 260 °C. Above 260 °C, the sample starts to decompose. A slightly different behavior was reported by Wuttke et al.[14] using a helium flow: at 150 °C, they observed only the removal of physisorbed water, while the water directly bonded to the $Fe_3O$ clusters was fully desorbed at 200 °C. Moreover, the removal of X is far less effective in a helium flow than in dynamic vacuum.[4] Also X plays a role in the thermal behavior of $Fe_3O$ samples: the removal of only 4−5% of Fe−X was reported at 250 °C for a MIL-100(Fe) (X = 20% Cl, OH, trimesate) sample.[9,18] Different


https://doi.org/10.1021/acs.inorgchem.1c01044
Inorg. Chem. 2021, 60, 11813−11824

**Table 1. Water Adsorption on $Fe_3O$ Clusters Optimized at the UM06-L/def2-TZVP Level in Their Ground Spin State ($S$)[a]**

| model | $2S+1$ | $d(Fe-O_{H_2O})$ | $d(Fe-O_c)$ | $\Delta E_{H_2O}$ | $\Delta E^c_{H_2O}$ | $\Delta H^c_{H_2O}$ | $\Delta G^c_{H_2O}$ |
|---|---|---|---|---|---|---|---|
| | | | $Fe_3O$ | | | | |
| $1H_2O$ | 15 | 2.169 | 1.921 | −86.9 | −81.8 | −73.8 | −29.2 |
| $2H_2O$ | 15 | 2.185 | 1.919 | −85.5 | −79.5 | −72.1 | −30.6 |
| | | 2.184 | 1.919 | | | | |
| $3H_2O$ | 15 | 2.201 | 1.913 | −79.5 | −73.5 | −65.2 | −19.5 |
| | | 2.200 | 1.907 | | | | |
| | | 2.204 | 1.906 | | | | |
| | | | $Fe_3O$-Cl | | | | |
| $1H_2O$ | 16 | 2.196 | 1.891 | −83.4 | −77.0 | −69.6 | −27.3 |
| $2H_2O$ | 16 | 2.217 | 1.879 | −77.4 | −71.2 | −63.6 | −20.6 |
| | | 2.221 | 1.883 | | | | |
| | | | $Fe_3O$-OH | | | | |
| $1H_2O$ | 16 | 2.198 | 1.888 | −82.9 | −76.6 | −69.1 | −25.4 |
| $2H_2O$ | 16 | 2.223 | 1.876 | −76.0 | −69.8 | −61.6 | −17.1 |
| | | 2.223 | 1.880 | | | | |

[a]All of the reported values refer only to the iron sites coordinating a water molecule. The distance of the reacting iron from the water O $d(Fe-O_{H_2O})$ and from the central O of the $Fe_3O$ cluster $d(Fe-O_c)$ are also reported (in angstroms). The BSSE-corrected adsorption energy $\Delta E^c_{H_2O}$, adsorption enthalpy $\Delta H^c_{H_2O}$, and adsorption Gibbs free energy $\Delta G^c_{H_2O}$ are reported in kilojoules per mole. The value not corrected for the BSSE is also shown for the energy ($\Delta E_{H_2O}$). $H$ has been calculated at 1013.25 mbar and 25 °C.

clusters have to be adopted to model MIL-100(Fe) treated at different temperatures $T$ in degrees Celsius [in the following MIL-100(Fe)-$T$C] because the type and number of adsorbed species (X and Z) on the metal node are different. Considering the information reported in refs 4 and 5, we have used $Fe_3O$-Cl·$2H_2O$, $Fe_3O$-OH·$2H_2O$, and $Fe_3O$·$3H_2O$ to model MIL-100(Fe) samples treated at $T \leq 100$ °C. $Fe_3O$-Cl·$1H_2O$, $Fe_3O$·$1H_2O$, $Fe_3O$-OH·$1H_2O$, and $Fe_3O$·$2H_2O$ have been used for MIL-100(Fe)-120C. For MIL-100(Fe) treated at 150, 200, and 250 °C, the models used have been the same ($Fe_3O$-Cl, $Fe_3O$-OH, and $Fe_3O$), with only the proportion of the species being different (e.g., $Fe_3O$ represents 2% of all of the metal nodes in MIL-100(Fe)-150C and 40% of the metal nodes in MIL-100(Fe)-250C treated in a dynamic vacuum for 40 h).

The ground-state electronic configuration for all of the systems has the three iron centers in high spin states. However, the most stable configuration for the $Fe_3O$-Cl, $Fe_3O$-OH, and $Fe_3O$ is not the highest possible spin state for the cluster (HS) but the "broken-symmetry" solution (BS) where two high-spin Fe(III) centers couple antiferromagnetically. Although the BS energetics would be more accurate,[9,41] the corresponding wave function is not a spin eigenfunction nor does it have the correct spin density. Moreover, the BS solution is strongly dependent on the initial guess, hindering both the reproducibility of the BS results and the comparison among different studies. Following a common strategy,[41−43] we modeled all of the clusters considering the $Fe_3O$ node in HS. In general, the difference in energy between the HS and BS is 20−30 kJ mol$^{-1}$. For details on this choice, see the discussion reported in previous studies.[8,9,31] Coordination of the adsorbates can cause a change in the ground spin state of the iron centers. This has been evaluated for a range of spin states starting from the HS value of the bare triiron oxo-centered clusters to determine the most stable spin state.

The calculations indicate that each iron center can coordinate only one adsorbate molecule: when more than one molecule is adsorbed on one metal node, each molecule is coordinated to a different metal site of the metal node. The highest coverage corresponds to filling of the position left free by X and Z (marked with green spheres in Figure 1a). This agrees with the available IR experiments on CO and NO adsorption that show the formation of monocarbonyls and mononitrosyls only.[5,14] Only in the NO case, forcing the formation of a Fe···2NO complex brings displacement of the carboxylate groups. This complex is a local minimum, but it is less stable than the mononitrosyl complex by 10 kJ mol$^{-1}$. Such a displacement is possible in a cluster model where no geometrical constraints were used in the optimization, while it is unlikely to happen in the MOF structure because of the framework constraints and because of the large cluster distortion, at least at subatmospheric NO pressures considered in the experiments.[24] Accordingly, the experimental spectra do not show the formation of dinitrosyls.[24]

**$H_2O$ Adsorption.** The water adsorption on $Fe_3O$, $Fe_3O$-OH, and $Fe_3O$-Cl clusters was studied by increasing the number of water molecules until all of the open iron sites are coordinated. The results are reported in Table 1, Figure 2, and Table S6.

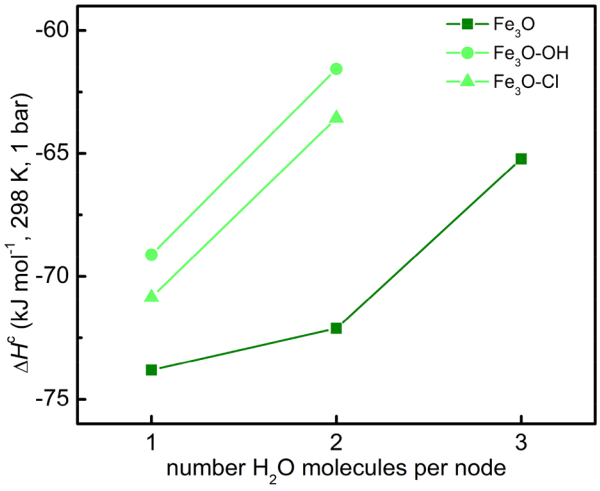


**Figure 2.** Enthalpy of water adsorption on $Fe_3O$ clusters, $\Delta H^c$, as a function of the water coverage, obtained at the UM06-L/def2-TZVP level for the three models of the fully dehydrated MOFs (treatment temperature ≥150 °C): $Fe_3O$ (green squares), $Fe_3O$-Cl (light-green triangles), and $Fe_3O$-OH (light-green circles).


https://doi.org/10.1021/acs.inorgchem.1c01044
Inorg. Chem. 2021, 60, 11813−11824

**Table 2. CO Adsorption on $Fe_3O$ Clusters**[a]

| model | $2S+1$ | $d$ (Fe−$C_{CO}$) | ∠Fe−C−O | $\Delta E_{CO}$ | $\Delta E^c_{CO}$ | $\Delta H^c_{CO}$ | $\Delta G^c_{CO}$ | $\Delta\tilde{\nu}_{CO}$ |
|---|---|---|---|---|---|---|---|---|
| | | | | $Fe_3O$ | | | | |
| 1CO | 15 | 2.316 | 178 | −46.5 | −49.6 | −45.3 | −7.8 | 29 |
| 2CO | 15 | 2.385 | 178 | −43.4 | −46.4 | −41.9 | −3.5 | 45 |
| | | 2.385 | 178 | | | | | 45 |
| 3CO | 15 | 2.412 | 179 | −41.8 | −44.8 | −40.2 | −1.7 | 48 |
| | | 2.408 | 179 | | | | | 47 |
| | | 2.412 | 180 | | | | | 46[b] |
| | | | | $Fe_3O{\cdot}1H_2O$ | | | | |
| 1CO | 15 | 2.383 | 178 | −44.6 | −47.6 | −43.3 | −5.6 | 45 |
| 2CO | 15 | 2.416 | 179 | −40.7 | −37.8 | −33.2 | 4.9 | 44 |
| | | 2.416 | 179 | | | | | 43 |
| | | | | $Fe_3O{\cdot}2H_2O$ | | | | |
| 1CO | 15 | 2.426 | 180 | −39.9 | −37.0 | −32.7 | 5.0 | 44 |
| | | | | $Fe_3O$-Cl | | | | |
| 1CO | 16 | 2.428 | 180 | −42.8 | −39.6 | −35.3 | 2.5 | 51 |
| 2CO | 16 | 2.448 | 180 | −39.0 | −35.9 | −31.5 | 5.8 | 46 |
| | | 2.451 | 179 | | | | | 45 |
| | | | | $Fe_3O$-Cl$\cdot1H_2O$ | | | | |
| 1CO | 16 | 2.462 | 180 | −38.7 | −35.6 | −31.4 | 5.7 | 44 |
| | | | | $Fe_3O$-OH | | | | |
| 1CO | 16 | 2.425 | 180 | −42.1 | −38.9 | −34.6 | 3.8 | 50 |
| 2CO | 16 | 2.445 | 179 | −38.4 | −35.3 | −30.8 | 6.9 | 45 |
| | | 2.445 | 179 | | | | | 44 |
| | | | | $Fe_3O$-OH$\cdot1H_2O$ | | | | |
| 1CO | 16 | 2.456 | 179 | −37.7 | −34.6 | −30.3 | 7.9 | 43 |

[a]All of the values refer only to the iron sites coordinating a CO molecule. Clusters were optimized at the UM06-L/def2-TZVP level in their ground spin state ($S$). The distance of the reacting iron from the C of the CO molecule [$d$(Fe−$C_{CO}$) in angstroms] and the Fe···CO angle (∠Fe−C−O, in degrees) are also reported. The stretching frequency shift ($\Delta\tilde{\nu}_{CO}$ in reciprocal centimeters) is calculated from the gas-phase values ($\tilde{\nu}_{CO}$ = 2202 $cm^{-1}$). The BSSE-corrected adsorption energy $\Delta E^c_{CO}$, adsorption enthalpy $\Delta H^c_{CO}$, and adsorption Gibbs free energy $\Delta G^c_{CO}$ are reported in kilojoules per mole. The value not corrected for the BSSE is also shown for the energy ($\Delta E_{CO}$). $H$ and $G$ have been calculated at 1013.25 mbar and 25 °C. [b]Vibration involving only one CO molecule (made explicit only for the 2CO and 3CO complexes).

All of the values reported in Table 1 for the adsorption enthalpy $\Delta H^c_{H_2O}$ are within the range from −74 to −62 kJ $mol^{-1}$. The calculations show that $\Delta H^c_{H_2O}$ has only a slight dependence on the iron oxidation state [it increases upon going from Fe(II) to Fe(III)], while its dependence on the counteranion is negligible (it increases upon going from −Cl to −OH; Table 1 and Figure 2). The $\Delta H^c_{H_2O}$ value becomes less negative with coverage only where the adsorption of the last water molecule is concerned, by about 10 kJ $mol^{-1}$ less than the first one(s).

Jeremias et al.[6] determine the isosteric heat for water in MIL-100(Fe), after degassing the sample at 120 °C for 17 h. On the basis of refs 5 and 14, this sample should be mainly constituted of $Fe_3O$-X clusters, with some residual $Fe_3O$-X$\cdot1H_2O$ and a negligible amount of $Fe_3O$. The lowest coverage values reported in ref 6 correspond to about two water molecules per $Fe_3O$, and they are characterized by a heat of 90 ± 30 and 80 ± 20 kJ $mol^{-1}$. The isosteric heat then reaches a constant value of 60 ± 10 kJ $mol^{-1}$ for coverage ≥4 $H_2O/Fe_3O$. All of these experimental values are similar, considering the error bar. The values reported in Table 1 and Figure 1 agree with the experimental values and reproduce the small dependence on the coverage of the isosteric heat on MIL-100(Fe).

The vibrational bending modes of water, $\delta(H_2O)$, can be used to determine the oxidation state of the metal node: the calculations indicate that $\delta(H_2O)$ is shifted to lower wavenumbers if the cluster is in its oxidized form, while it is shifted to higher wavenumbers if it is reduced (Figure S3).

**CO Adsorption.** Relevant energetic, geometric, and spectroscopy parameters for all of the CO complexes are reported in Table 2, while additional parameters are listed in Tables S2 and S5.

CO is adsorbed end-on, C-side, in all of the complexes on the iron centers, with a linear geometry (Table 2 and Figure 3a). The enthalpy of adsorption, $\Delta H^c_{CO}$, spans a range from −45.3 to −30.3 kJ $mol^{-1}$, and it is lower for the $Fe_3O$ clusters than for the $Fe_3O$-OH and $Fe_3O$-Cl ones. Moreover, $\Delta H^c$ is almost independent on the coverage except for $Fe_3O{\cdot}1H_2O$, where an increase of 10 kJ $mol^{-1}$ is observed upon going from 1CO/$Fe_3O{\cdot}1H_2O$ to 2CO/$Fe_3O{\cdot}1H_2O$. The $\Delta H^c_{CO}$ values are all lower than the calculated adsorption enthalpies for water (Table 1). This is a valuable property for drug delivery because CO release can be triggered by water. Nevertheless, this is detrimental for CO capture because water would be preferably adsorbed over CO on $Fe_3O$-based MOFs. $\Delta\tilde{\nu}_{CO}$ is almost constant for all of the complexes in Table 2, with all of the values being between 43 and 51 $cm^{-1}$, with one outlier: the complex of one CO molecule with $Fe_3O$ ($\Delta\tilde{\nu}_{CO}$ = 29 $cm^{-1}$).

Yoon et al.[4] employed microcalorimetry to study CO adsorption on MIL-100(Fe)-100C and MIL-100(Fe)-250C at 30 °C for pressures from 0 to 150 mbar. Calorimetric values for CO adsorption on MIL-100(Fe)-150C are reported in ref 5. The analysis of these data shows that the heat of adsorption increases with the temperature used for the postsynthetic treatment. For MIL-100(Fe)-100C, the heat of adsorption was found to vary from −34.7 to −29.1 kJ $mol^{-1}$ for coverage as low as 0.013−


https://doi.org/10.1021/acs.inorgchem.1c01044
Inorg. Chem. 2021, 60, 11813−11824

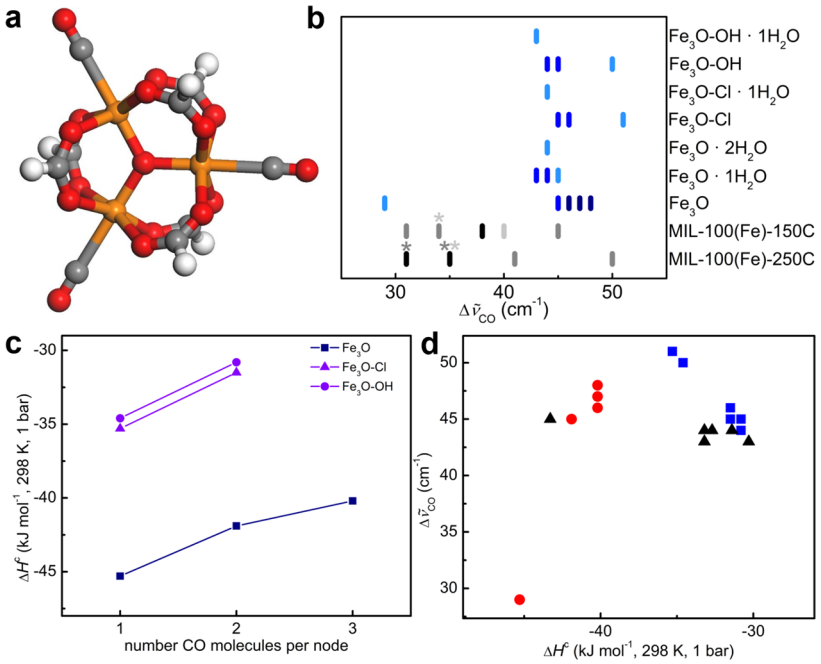


**Figure 3.** CO complexes on $Fe_3O$ clusters. (a) Optimized structure of $3CO/Fe_3O$. The color code is as in Figure 1. Results were obtained at the UM06-L/def2-TZVP level and are reported in Table 2. (b) CO vibrational shifts on $Fe_3O$, $Fe_3O$-OH, and $Fe_3O$-Cl for different degrees of hydration of the metal node. The colors differentiate different loadings of CO per metal node, and then the CO species that can be formed at different pressures. Color code: light blue, 1CO complexes; blue, 2CO; dark blue, 3CO. In all of the complexes, the minimum geometries show the formation of only monocarbonyl species. The formation of dicarbonyl or tricarbonyl is not allowed. The data in ref 5 for ∼zero (light-gray lines), low-to-middle (gray), and high (black) pressures, as in Table 3, for MIL-100(Fe)-150C and MIL-100(Fe)-250C are also reported. The asterisks indicate the bands that are also associated with the ∼0 (light gray) or low-to-middle (gray) coverage. (c) Enthalpy of adsorption on $Fe_3O$ clusters, $\Delta H^c$, as a function of the coverage on models for the fully dehydrated MOFs (treatment temperature ≥150 °C): $Fe_3O$, blue squares; $Fe_3O$-Cl, violet triangles; $Fe_3O$-OH, violet circles. (d) Dependence of the CO stretching frequency shift $\Delta\tilde{\nu}_{CO}$ on the adsorption enthalpy $\Delta H^c_{CO}$ for the clusters modeling $Fe_3O$-based materials treated at temperature lower (black triangles) or higher (blue squares, $Fe_3O$-Cl and $Fe_3O$-OH; red circles, $Fe_3O$) than 150 °C. Complexes with lower adsorption enthalpies correspond to species formed at lower equilibrium pressures and at higher temperatures in the experiments (Table 3).

0.027 CO per $Fe_3O$. The heat of adsorption increases to 38−40 kJ $mol^{-1}$ for MIL-100(Fe)-150C,[5] while for MIL-100(Fe)-250C, it goes from −50.2 kJ $mol^{-1}$ (at 0.047 CO per $Fe_3O$) to −39.5 kJ $mol^{-1}$ (at 0.26 CO per $Fe_3O$). This dependence was explained by the removal of an increasing number of X and Z from the clusters, and the present calculations support this hypothesis. In MIL-100(Fe)-100C, both X and Z are still coordinated to the $Fe_3O$ nodes (see section 3). Accordingly, these values are closer to the calculated $\Delta H^c_{CO}$ for all of the $Fe_3O$-X·$nH_2O$ clusters and for $Fe_3O{\cdot}2H_2O$ (Table 2). In MIL-100(Fe)-150C, Z is fully removed: CO can interact with open $Fe^{3+}$ sites.[5] The $\Delta H^c_{CO}$ values for CO complexes with $Fe_3O$-X clusters are close to the experimental values. In MIL-100(Fe)-250C, Z and X are desorbed from the metal nodes, allowing the formation of divalent iron centers.[4,5] This explains the higher heat of adsorption measured for this sample: Fe(II) sites stabilize the adsorbed CO by $\pi$ interaction, in addition to the $\sigma$-donor interaction with the $Fe^{3+}$ sites.[5] The calculated $\Delta H^c_{CO}$ values for the adsorption of the first CO molecule on $Fe_3O$ and $Fe_3O{\cdot}1H_2O$ are the closest values to the heat measured for CO adsorption on MIL-100(Fe)-250C.

CO adsorption on MIL-100(Fe) has been investigated by means of IR spectroscopy in previous works.[4,5,14] The experimental studies have discussed only the changes observed in the CO stretching frequency region. Additional bands associated with vibrational modes involving CO (e.g., the bending mode of Fe···CO) are expected in the spectral region below 800 $cm^{-1}$. The description of theoretical spectra in this range is reported in Figure S1. Yoon et al.[4] and Wuttke et al.[14] have studied it at room temperature in a flow of 10% CO in helium (Table 3) to determine how the CO surface species formed at a certain CO partial pressure change with the treatment temperature. Leclerc et al.[5] have investigated how the CO bands change with the coverage up to CO condensation: this allowed them to characterize all of the adsorption sites present on the MIL surface. Leclerc et al.[5] have recorded the spectra on MIL-100(Fe)-150C and MIL-100(Fe)-250C at −173 °C in static conditions and by increasing the pressure up to 0.53 mbar (Table 3).

The CO spectra reported in refs 4 and 14 show three bands, whose intensity changes with the treatment temperature: a band at 2189 $cm^{-1}$ is present also after treatments at $T$ < 150 °C, associated with CO on Fe(III) sites, and two bands at 2182 (or 2185) and 2173 $cm^{-1}$ gain significant intensity only after the reduction of Fe(III) to Fe(II). The intensity of the signals is slightly different in refs 4 and 14 likely because of a different thermal history of the two samples. In particular, the band at 2173 $cm^{-1}$ is dominant in the spectra of MIL-100-250C reported in ref 4, while in ref 14. the bands at 2173 and 2182 $cm^{-1}$ share the same intensity. Because these bands appear only after the formation of Fe(II) sites and they are not removed after prolonged outgassing at room temperature, they have been associated in refs 4, 5, and 14 with two different Fe(II) sites. In the crystallographic cell of MIL-100, all of the Fe(II) sites are equivalent: the presence of more than one Fe(II) site was explained by the presence of defects in the material. However, no signals typically associated with defects in MOFs[46] are visible in


https://doi.org/10.1021/acs.inorgchem.1c01044
Inorg. Chem. 2021, 60, 11813−11824

**Table 3. Review of Experimental CO Stretching Frequencies ($\tilde{\nu}_{CO}$) Recorded for CO Adsorption in MIL-100(Fe) Samples by IR spectroscopy[a]**

| material | treatment | $T_{IR}$ | $P_{IR}$ | $\tilde{\nu}_{CO}$[b] | $\Delta\tilde{\nu}_{CO}$ | original assignment |
|---|---|---|---|---|---|---|
| MIL-100(Fe)[4] | 100 °C, 12 h | 25 | 100[c] | 2190(l) | 47 | Fe(III)···CO |
| | 150 °C, 12 h | 25 | 100[c] | 2190(l) | 47 | Fe(III)···CO |
| | | | | 2182(s) | 39 | Fe(II)···CO |
| | | | | 2173(s) | 30 | Fe(II)···CO |
| | 200 °C, 12 h | 25 | 100[c] | 2190(s) | 47 | Fe(III)···CO |
| | | | | 2182 | 39 | Fe(II)···CO |
| | | | | 2173(s) | 30 | Fe(II)···CO |
| | 250 °C, 12 h | 25 | 100[c] | 2182(s) | 39 | Fe(II)···CO |
| | | | | 2173 | 30 | Fe(II)···CO |
| MIL-100(Fe)[14] | 100 °C, 12 h | 25 | 100[c] | 2189(l) | 46 | Fe(III)···CO |
| | 150 °C, 12 h | 25 | 100[c] | 2189(l) | 46 | Fe(III)···CO |
| | | | | 2182(s) | 39 | Fe(II)···CO |
| | 200 °C, 12 h | 25 | 100[c] | 2189(s) | 46 | Fe(III)···CO |
| | | | | 2182 | 39 | Fe(II)···CO |
| | | | | 2173(s) | 30 | Fe(II)···CO |
| | 250 °C, 12 h | 25 | 100[c] | 2182 | 39 | Fe(II)···CO |
| | | | | 2175 | 32 | Fe(II)···CO |
| MIL-100(Fe)[5] | 150 °C, 12 h | −173 | ∼0.0 | 2175(s) | 40 | Fe(II)···CO |
| | | | | 2169(l) | 34 | Fe(II)···CO |
| | | | low[d] | 2192(l) | 57 | Fe(III)···CO |
| | | | | 2169 | 34 | Fe(II)···CO |
| | | | medium[d] | 2180(l) | 45 | Fe(III)···CO |
| | | | | 2166(s) | 31 | Fe(II)···CO |
| | | | high[d] | 2173(l) | 38 | Fe(III)···CO |
| | | | | 2138 | 3 | physisorbed CO |
| MIL-100(Fe)[5] | 250 °C, 12 h | −173 | ∼0.0 | 2170 | 35 | Fe(II)···CO |
| | | | low[d] | 2185 | 50 | Fe(III)···CO |
| | | | | 2170 | 35 | Fe(II)···CO |
| | | | medium[d] | 2176 | 41 | Fe(III)···CO |
| | | | | 2166 | 31 | Fe(II)···CO |
| | | | high[d] | 2170(s) | 35 | Fe(III)···CO |
| | | | | 2166 | 31 | Fe(II)···CO |
| | | | | 2138 | 3 | physisorbed CO |

[a]The treatment protocol and the temperature ($T_{IR}$) and pressure ($P_{IR}$) conditions used in the IR measurements are reported. For each frequency, the assignment reported in the original paper is also shown. Reference values for CO in the gas phase in a microporous matrix used for the calculation of the CO stretching frequency shift ($\Delta\tilde{\nu}_{CO}$): 2135 $cm^{-1}$ at −173 °C[44,45] and 2143 $cm^{-1}$ at 25 °C.[45] Frequencies ($cm^{-1}$), temperatures (°C), pressures (mbar). [b](w) = weak, (s) = shoulder, (l) = large. [c]10% CO in a helium flow. [d]Set of spectra recorded at increasing pressures: low and medium pressures are relative values with respect to the highest values used in ref 5 (0.53 mbar, high).

the spectral regions typical of −OH stretching frequencies and of carboxylate absorption.[5]

The set of spectra recorded at −173 °C is used to follow CO adsorption up to the filling of all of the open iron sites (Table 3).[5] The description of the bands for the intermediate coverage is the same as that reported at room temperature: the main difference is associated with the position of the bands, shifted of about −6 $cm^{-1}$ as an effect of the temperature.[44,45] At the highest CO coverage, when all of the open metal sites are coordinated, the CO spectrum is composed of a large single band centered at 2173 $cm^{-1}$ ($\Delta\tilde{\nu}_{CO}$ = 38 $cm^{-1}$) for MIL-100(Fe)-150C, while it is shifted to 2166 $cm^{-1}$ ($\Delta\tilde{\nu}_{CO}$ = 31 $cm^{-1}$) for MIL-100(Fe)-250C.

The calculations can reproduce the evolution of CO spectra with the coverage and differences observed with different treatment temperatures in the experiments. On the basis of the DFT results, we expect that, with increasing CO pressure in MIL-100(Fe)-150C/200C/250C, the first sites to be occupied by CO molecules will be the Fe(II) sites, followed by the Fe(III) sites in $[Fe^{II}Fe^{III}_2(\mu_3\text{-}O)]^{6+}$ metal nodes, while Fe(III) in $[Fe^{III}_3X(\mu_3\text{-}O)]^{6+}$ will be coordinated only at the highest pressures (Table 2 and Figure 3c,d). The calculated CO adsorption enthalpy of the Fe(III) sites in $Fe_3O$-X nodes is less exothermic by 10 kJ $mol^{-1}$ than that for Fe(III) sites in a reduced metal node. Moreover, the adsorption of a second (and of a third) CO on 1CO/$Fe_3O$ is expected to start before all 1CO/$Fe_3O$ species are formed because 1CO/$Fe_3O$ and 2CO/$Fe_3O$ have similar $\Delta H^c_{CO}$ values.

The calculated $\Delta\tilde{\nu}_{CO}$ for 1CO complexes is significantly different if the metal node is fully activated ($Fe_3O$, +29 $cm^{-1}$) or if it is coordinating the counteranion ($Fe_3O$-Cl or $Fe_3O$-OH, ∼50 $cm^{-1}$) and/or a water molecule (∼45 $cm^{-1}$). These shifts are close to those observed for the spectra recorded at the lowest coverage on samples degassed at different $T$ values (Table 3). In particular, the models are able to reproduce the $\Delta\tilde{\nu}_{CO}$ values for both Fe(II)···CO and Fe(III)···CO complexes observed experimentally (35 and 50 $cm^{-1}$, respectively).[5] The results obtained for $Fe_3O$-Cl and $Fe_3O$-OH are fully comparable, suggesting that the IR spectra of CO cannot help to distinguish between clusters with different X.


https://doi.org/10.1021/acs.inorgchem.1c01044
Inorg. Chem. 2021, 60, 11813−11824

Table 4. NO Adsorption on $Fe_3O$ Clusters Optimized at the UM06-L/def2-TZVP Level in Their Ground Spin State ($S$)[a]

| model | $2S+1$ | $d$ (Fe−$N_{NO}$) | ∠Fe−N−O | $\Delta E_{NO}$ | $\Delta E^c_{NO}$ | $\Delta H^c_{NO}$ | $\Delta G^c_{NO}$ | $\Delta\tilde{\nu}_{NO}$ |
|---|---|---|---|---|---|---|---|---|
| | | | | $Fe_3O$ | | | | |
| 1NO | 14 | 1.802 | 179 | −119.1 | −113.7 | −108.3 | −68.7 | −57 |
| 2NO | 13 | 1.807 | 167 | −62.2 | −58.3 | −54.5 | −13.8 | −71[b] |
| | | 2.266 | 124 | | | | | −1[b] |
| 3NO | 12 | 1.810 | 163 | −56.3 | −52.5 | −48.6 | −8.8 | −82[b] |
| | | 2.292 | 122 | | | | | −11 |
| | | 2.284 | 123 | | | | | 3 |
| | | | | $Fe_3O{\cdot}1H_2O$ | | | | |
| 1NO | 14 | 1.809 | 164 | −113.2 | −110.7 | −105.5 | −66.4 | −73 |
| 2NO | 13 | 1.814 | 160 | −56.1 | −52.3 | −48.9 | −9.9 | −85 |
| | | 2.294 | 123 | | | | | −2 |
| | | | | $Fe_3O{\cdot}2H_2O$ | | | | |
| 1NO | 14 | 1.817 | 156 | −101.6 | −99.2 | −93.6 | −52.7 | −90 |
| | | | | $Fe_3O$-Cl | | | | |
| 1NO | 15 | 2.270 | 124 | −64.4 | −60.4 | −56.4 | −15.8 | 5 |
| 2NO | 16 | 2.280 | 123 | −27.3 | −21.4 | −17.5 | 18.0 | 5[b] |
| | | 2.597 | 129 | | | | | 24[b] |
| 2NO | 14 | 1.774 | 169 | −5.7 | −2.7 | 0.6 | 41.1 | 6 |
| | | 2.663 | 126 | | | | | −32 |
| 2NO | 12 | 1.775 | 178 | −28.5 | −25.6 | −20.2 | 26.9 | 5 |
| | | 2.662 | 124 | | | | | −32 |
| | | | | $Fe_3O$-Cl$\cdot 1H_2O$ | | | | |
| 1NO | 15 | 2.296 | 123 | −58.8 | −54.9 | −50.6 | −9.5 | 3 |
| | | | | $Fe_3O$-OH | | | | |
| 1NO | 15 | 2.269 | 124 | −63.4 | −59.4 | −55.4 | −15.2 | 4 |
| 2NO | 16 | 2.277 | 123 | −26.9 | −23.1 | −19.1 | 17.3 | 3[b] |
| | | 2.602 | 129 | | | | | 24[b] |
| 2NO | 14 | 2.670 | 126 | −5.0 | 0.9 | 4.1 | 45.5 | −1 |
| | | 1.775 | 168 | | | | | −35 |
| 2NO | 12 | 2.316 | 124 | −28.1 | −22.2 | −17.0 | 31.3 | 8 |
| | | 1.760 | 177 | | | | | −7 |
| | | | | $Fe_3O$-OH$\cdot 1H_2O$ | | | | |
| 1NO | 15 | 2.298 | 123 | −57.1 | −53.2 | −49.0 | −9.6 | 2 |

[a]All of the values reported in this table refer only to the iron sites coordinating a NO molecule. The distance of the reacting iron from the nitrogen of the NO molecule [$d$(Fe−$N_{NO}$) in angstroms] and the Fe···NO angle (∠Fe−N−O, in degrees) are also reported. The stretching frequency shift ($\Delta\tilde{\nu}_{NO}$ in reciprocal centimeters) is calculated from the gas-phase values ($\tilde{\nu}_{NO}$ = 1979 $cm^{-1}$). The BSSE-corrected adsorption energy $\Delta E^c_{NO}$, adsorption enthalpy $\Delta H^c_{NO}$, and adsorption Gibbs free energy $\Delta G^c_{NO}$ are reported in kilojoules per mole. The value not corrected for the BSSE is also shown for the energy ($\Delta E_{NO}$). $H$ has been calculated at 1013.25 mbar and 25 °C. [b]Vibration involving mainly one NO molecule (made explicit only for 2NO and 3NO complexes).

For intermediate coverage, the experimental spectra show the presence of a doublet, where only the relative intensity of the peaks is dependent on $T$, while the position of the peaks is independent. The two peaks have been assigned to Fe(II)···CO ($\Delta\tilde{\nu}_{CO}$ = 31 $cm^{-1}$) and Fe(III)···CO (41 $cm^{-1}$).[5] The calculations suggest an alternative assignment for the higher-frequency band of the doublet. When two CO molecules are adsorbed on the same metal node, each vibrational mode in the CO spectral region is associated with the combination of the modes of the two CO molecules, that is, to the asymmetric or the symmetric stretching of the two CO molecules. For 3CO/$Fe_3O$, the three modes are associated with the symmetric stretching of all of the CO molecules ($\Delta\tilde{\nu}_{CO}$ = 46 $cm^{-1}$), the asymmetric C−O stretching of the two Fe···CO moieties (47 $cm^{-1}$), and the C−O stretching of Fe···CO (48 $cm^{-1}$), respectively. The predicted shift for modes associated with the 2CO and 3CO complexes is 45 $cm^{-1}$, independent of the metal node. This value is very close to the higher-frequency peak of the doublet (41 $cm^{-1}$) that we assign, based also on the discussion above, to the formation of 2CO complexes on $[Fe^{II}Fe^{III}_2(\mu_3\text{-}O)]^{6+}$ metal nodes. The band at 31 $cm^{-1}$ is assigned to 1CO complexes on the same nodes ($Fe_3O$).

The calculations predict that the shifts on the different $Fe_3O$ nodes become more and more similar with increasing coverage: all of the IR bands should evolve toward a single band at higher pressures (Figure 3b). Although the predicted shift is slightly higher than the experimental one (48−44 vs 38−35 $cm^{-1}$), the models catch correctly the evolution of the CO spectra with the pressure reported in ref 5. The larger shift obtained in the calculations is associated with a similar description of the three Fe···CO in 3CO/$Fe_3O$ (Table 2 and Figure 3a). The three CO−Fe distances are very similar, and the three iron sites have similar partial charges, which is not surprising because DFT tends to delocalize the electronic density.

**NO Adsorption.** Relevant electronic, structural, and energetic parameters of the NO complexes on $Fe_3O$, $Fe_3O$-OH, and $Fe_3O$-Cl, considering different degrees of hydration, are reported in Tables 4, S3, and S4.

NO adsorbs on $Fe_3O$ clusters with a bent geometry in most of the cases (see Figure 4a and ∠Fe−N−O values in Table 4). The calculated enthalpy of NO adsorption, $\Delta H^c_{NO}$, is strongly


https://doi.org/10.1021/acs.inorgchem.1c01044
Inorg. Chem. 2021, 60, 11813−11824

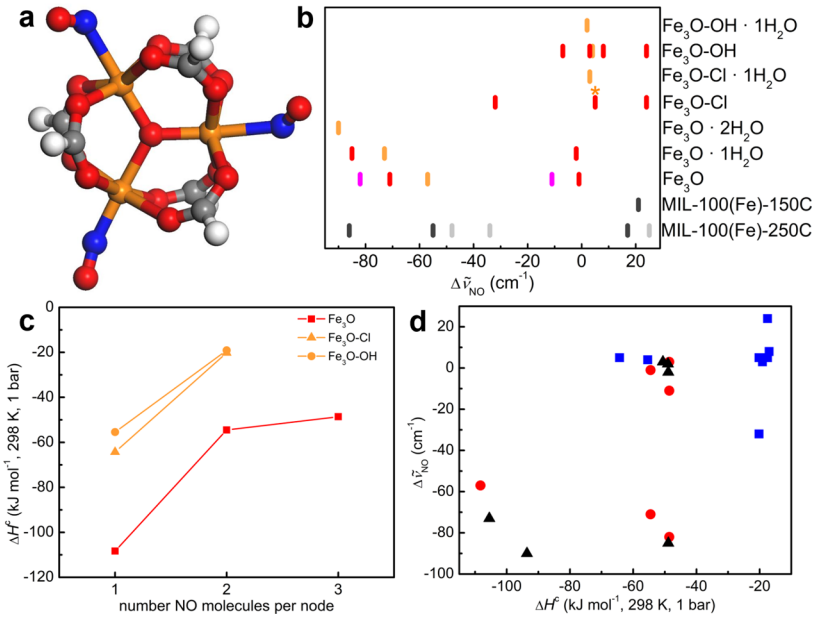


**Figure 4.** NO complexes on $Fe_3O$ metal nodes treated at different temperatures. Results were obtained at the UM06-L/def2-TZVP level. (a) Optimized structure of $3NO/Fe_3O$. Color code: red, oxygen; gray, carbon; blue, nitrogen; orange, iron; white, hydrogen. (b) NO vibrational shifts on $Fe_3O$, $Fe_3O$-OH, and $Fe_3O$-Cl for different degrees of hydration of the metal node for the ground-state structures. The colors differentiate different loadings of NO per metal node, and then the NO species can be formed at different pressures. Color code: orange, 1NO complexes; red, 2NO; magenta, 3NO. In all of the complexes, the minimum geometries show the formation of only mononitrosyl species. For the $Fe_3O$-Cl/2NO complex, the data shown are for both the $2S + 1 = 16$ and 12 complexes. The asterisk indicates that this band is also associated with the corresponding 1NO complex (Table 4). The experimental data in ref 24 for MIL-100(Fe)-150C and MIL-100(Fe)-250C at 25 °C (gray lines) and −53 °C (black lines) are also reported. (c) Enthalpy of NO adsorption on $Fe_3O$ clusters, $\Delta H^c$, as a function of the coverage, as obtained on clusters modeling the fully dehydrated MOFs (treatment temperature ≥150 °C): $Fe_3O$, red squares; $Fe_3O$-OH, orange circles; and $Fe_3O$-Cl, orange triangles. (d) Dependence of the shift of the NO stretching frequency $\Delta\tilde{\nu}_{NO}$ on the adsorption enthalpy $\Delta H^c_{NO}$ for the clusters modeling $Fe_3O$-based materials treated at temperature lower (black triangles) or higher than 150 °C (blue squares, $Fe_3O$-Cl; red circles, $Fe_3O$). Complexes with lower adsorption enthalpies correspond to species formed at lower equilibrium pressures and higher temperature in the experimental spectra (Table 5).

dependent on the NO coverage and on the oxidation state of iron (Table 4 and Figure 4d), unlike CO, for which $\Delta H^c_{CO}$ is independent of the coverage and only slightly decreasing with the reduction of the metal node (Table 2 and Figure 3c). $\Delta H^c_{NO}$ for 1NO complexes spans a range from −108 to −94 kJ mol$^{-1}$ on the reduced clusters, while for the oxidized cluster, it is halved (−64 kJ mol$^{-1}$ for $Fe_3O$-Cl and −51 kJ mol$^{-1}$ for $Fe_3O$-Cl·$1H_2O$). The adsorption of a second NO is by far less exothermic than the first one, with $\Delta H^c_{NO}$ being −50 kJ mol$^{-1}$ for the reduced clusters and −20 kJ mol$^{-1}$ for the oxidized ones. Although no experimental values are reported for the energetics of NO adsorption, Eubank et al.[24] have studied the competitive adsorption of water in an NO-loaded MIL-100(Fe)-250C(Fe) using IR spectroscopy. They verified by using IR spectroscopy that NO is not fully released at room temperature after switching from a dry to a wet helium flow. Our calculations agree with these observations: the calculated adsorption Gibbs free energy for $Fe_3O$ is lower than that calculated for water for the first NO (Tables 1 and 4), while it is higher than water for the second NO. The calculations also indicate that $\Delta G^c_{NO}$ for $Fe_3O$-Cl is always higher than $\Delta G^c_{H_2O}$. These results are an example of the importance of the temperature used in the postsynthetic treatment. For drug delivery, an $Fe_3O$-based degassed at ≤150 °C before to be loaded with NO will fully release NO after contact with a water-rich medium, while a MOF treated at ≥150 °C would allow a gradual release in time of NO, with a large amount of NO delivered immediately, followed by a slow desorption due to the gradual substitution of NO by water. MOFs showing a larger affinity for NO than for $H_2O$ have also been suggested for the environmental removal of NO.[47] The treatment temperature will have an important effect also on NO capture: $Fe_3O$-based MOFs treated at ≤150 °C have $\Delta G^c_{NO} > \Delta G^c_{H2O}$, and then they will not be able to capture NO in wet streams. The smaller $\Delta G^c_{NO}$ than $\Delta G^c_{H_2O}$ of $Fe_3O$-based MOFs treated at ≥150 °C would allow one to maintain good selectivity for NO also in wet gas streams, although their capacity will be limited to 1NO molecule per reduced $Fe_3O$ node.

The calculated $\Delta\tilde{\nu}_{NO}$ is strongly dependent on the oxidation state of iron (Table 4 and Figure 4b,d). For a description of the spectra in the region below 800 cm$^{-1}$, see the Supporting Information and Figure S2. For 1NO complexes, $\Delta\tilde{\nu}_{NO}$ spans from −57 to −90 cm$^{-1}$ if adsorbed on a reduced cluster, while it is +5 cm$^{-1}$ on oxidized clusters. A vibrational shift smaller than −70 cm$^{-1}$ is in general associated with a bent geometry, that is, with Fe−N−O angles (∠Fe−N−O) significantly different from 180°.[19,50] The calculations can model this behavior (Figure 4a and Table S3). When the loading (2NO and 3NO complexes) is increased, a different evolution of the bands is predicted for the oxidized and reduced clusters. For the reduced ones, two bands are predicted: one band almost corresponds with the gas-phase value, and a second one is shifted to lower wavenumbers with respect to the 1NO complex. For $2NO/Fe_3O$-Cl, two spin states are calculated to be isoenergetic: $2S + 1 = 16$ and 12 (Table 4). These spin states have different vibrational shifts, a doublet at 5 and 24 cm$^{-1}$ for $2S + 1 = 16$ and a doublet at 5 and −32 cm$^{-1}$ for $2S + 1 = 12$. For the reduced clusters, each vibrational mode is associated mainly with the stretching of a single NO molecule in 2NO complexes (Table 4), unlike for the $Fe_3O$-Cl-based


https://doi.org/10.1021/acs.inorgchem.1c01044
Inorg. Chem. 2021, 60, 11813−11824

**Table 5. Review of the Experimental Stretching Frequencies Recorded for NO Adsorbed in Different $Fe_3O$-Based MOFs by IR Spectroscopy ($\tilde{\nu}_{NO}$)[a]**

| material | treatment | $T_{IR}$ | $P_{IR}$ | $\tilde{\nu}_{NO}$[b] | $\Delta\tilde{\nu}_{NO}$ | original assignment |
|---|---|---|---|---|---|---|
| MIL-100(Fe)[24] | 150 °C | 25 | 25 | | | |
| | | −53 | 25 | 1897 | 21 | Fe(III)···NO |
| MIL-100(Fe)[24] | 250 °C | 25 | 25 | 1893(w) | 17 | Fe(III)···NO |
| | | | | 1821 | −55 | Fe(II)···NO |
| | | | | 1807 | −69 | Fe(II)···NO |
| | | −53 | 25 | 1893 | 17 | Fe(III)···NO |
| | | | | 1821 | −55 | Fe(II)···NO |
| | | | | 1790 | −86 | Fe(II)···NO |
| MIL-127(Fe) or PCN-250[24] | 250 °C | 25 | 25 | 1818 | −58 | Fe(II)···NO |
| | | | | 1795 | −81 | Fe(II)···NO |
| | | −53 | 25 | 1893 | 17 | Fe(III)···NO |
| | | | | 1818(s) | −58 | Fe(II)···NO |
| | | | | 1785(w) | −91 | Fe(II)···NO |
| MIL-100(Fe)[14] | 100 °C, 12 h | 25 | 10[c] | 1901 | 25 | Fe(III)···NO |
| | 150 °C, 12 h | 25 | 10[c] | 1901 | 25 | Fe(III)···NO |
| | | | | 1842(s) | −34 | Fe(II)···NO |
| | | | | 1828(w) | −48 | Fe(II)···NO |
| | 200/250 °C, 12 h | 25 | 10[c] | 1901 | 25 | Fe(III)···NO |
| | | | | 1842 | −34 | Fe(II)···NO |
| | | | | 1828 | −48 | Fe(II)···NO |
| MIL-100(Fe)[48] | 250 °C, 12 h | 25 | unknown | 1850(s) | −26 | Fe(II)···NO |
| | | | | 1825 | −51 | Fe(II)···NO |
| | | | | 1813 | −63 | Fe(II)···NO |
| Fe(BTC)(Fe)[48] | 250 °C, 12 h | 25 | unknown | 1850(s) | −26 | Fe(II)···NO |
| | | | | 1813(w) | −63 | Fe(II)···NO |
| MIL-88(Fe)A and MIL-88(Fe)-2OH[49] | 150 °C, 3 h | 25 | 1−67 | 1898 | 22 | Fe(III)···NO |
| | | | | 1813 | −63 | Fe(II)···NO |
| | | | 1000 | 1898 | 22 | Fe(III)···NO |
| | | | | 1845(w) | −31 | physisorbed NO |
| | | | | 1813(s) | −63 | Fe(II)···NO |
| MIL-88(Fe)B[49] | 80 °C, 3 h | 25 | 1−67 | 1898 | 22 | Fe(III)···NO |
| | | | 1000 | 1898 | 22 | Fe(III)···NO |
| | | | | 1870(s) | −6 | Fe(III)···ON |
| | | | | 1852(w) | −24 | physisorbed NO |
| MIL-88(Fe)B-$NO_2$[49] | 150 °C, 3 h | 25 | 1−1000 | 1900 | 24 | Fe(III)···NO |
| | | | | 1853(w) | −23 | physisorbed NO |

[a]The treatment protocol and the temperature ($T_{IR}$) and pressure ($P_{IR}$) conditions at which the band appears during the IR measurement are reported. For each frequency, the assignment reported in the original paper is also shown. Reference value for NO in the gas phase: 1876 $cm^{-1}$. Frequencies ($cm^{-1}$), temperatures (°C), and pressures (mbar). [b](w) = weak, (s) = shoulder, (l) = large. [c]1% NO in a helium flow.

clusters, where each mode involves both NO molecules (asymmetric and symmetric stretching modes). In 3NO/$Fe_3O$ complexes (Figure 4a), the three IR bands are associated with the symmetric and asymmetric stretching of the two NO in Fe(III)···NO (3 and −11 $cm^{-1}$, respectively) and to the N−O stretching in Fe(II)···NO (−82 $cm^{-1}$). This can be explained with the lower similarities of the Fe···NO species in $Fe_3O$ than in $Fe_3O$-Cl clusters because of the presence of Fe(II) species in the former able to engage a stronger interaction with NO species than Fe(III) sites.

Several IR studies reported NO adsorption on $Fe_3O$-based MOFs (see refs 14, 24, 48, and 49). Their results are summarized in Table 5. The experimental $\Delta\tilde{\nu}_{NO}$ assigned to NO···Fe(II) complexes in MIL-100(Fe)-250C agrees with the value calculated for 1NO/$Fe_3O$: −55 versus −57 $cm^{-1}$, respectively. The shift calculated for the adsorption of the first NO molecule on the oxidized cluster is very small (3−5 $cm^{-1}$), that is, almost indistinguishable from the gas-phase value. The signal of Fe(III)···NO complexes is associated with bands at ∼1895 $cm^{-1}$ (+20 $cm^{-1}$), a shift larger than the one predicted in the calculations. Nevertheless, there is a contradiction between the experimental results reported for IR and volumetric experiments. IR experiments either failed to detect NO adsorption on fully oxidized materials [e.g., MIL-100(Fe)-150C] at room temperature or obtained signals with very small intensity at ∼1895 $cm^{-1}$,[14,24] a symptom of a small interaction energy of NO with Fe(III) sites. Volumetric measurements indicate a large NO adsorption on the same materials under the same conditions.[24] Moreover, the volumetric measurements showed that NO can only be partially desorbed, indicating a strong interaction with the material that cannot be explained only by the presence of 2% Fe(II) sites.[24] The results reported in Table 4 explain this apparent contradiction. The Q band of NO in the gas phase is present in the experimental IR spectrum. The detection of bands slightly shifted from the gas-phase value is then difficult because these bands can be hidden behind the gas-phase absorption. The signals associated with 1NO/$Fe_3O$-Cl complexes, if not too intense, can be confused with the gas-phase


https://doi.org/10.1021/acs.inorgchem.1c01044
Inorg. Chem. 2021, 60, 11813−11824

signals in the experimental spectrum. This can also be the reason why none of the experimental shifts reported in Table 5 are close to zero. This observation can be useful also for the IR characterization of other materials using NO as a probe molecule, in order to avoid that signals associated with Fe(III) sites go unnoticed. The signal at 20 $cm^{-1}$ associated with a general Fe(III)···NO complex is assigned based on the present calculations to the second adsorbed molecule in $2NO/Fe_3O$-Cl clusters, having $2S + 1 = 16$. The bands observed in the −24 to −34 $cm^{-1}$ range were previously assigned to physisorbed NO[49] or the Fe(II)···NO complex.[14] The calculations suggest an alternative assignment, namely, the N−O stretching frequency of the second adsorbed molecule in $2NO/Fe_3O$-Cl clusters, having $2S + 1 = 12$.

No experimental spectra for the full coverage of iron sites by NO molecules have been reported, and they cannot thus be used to benchmark the evolution of the spectra predicted by the calculations. These results suggest that the NO spectra on MOFs treated at ≥150 °C are composed of three families of bands associated with $3NO/Fe_3O$ and $2NO/Fe_3O$-Cl complexes (Figure 4b). Unlike CO, characterized by a single broad band at higher CO/Fe coverage, NO can differentiate the different $Fe_3O$ nodes even at NO/Fe ∼ 1 and is thus a more suitable molecular probe to verify the efficacy of thermal treatments of $Fe_3O$-based MOFs.

## 4. CONCLUSIONS

Postsynthesis thermal treatments are effective ways to modify the performance of $Fe_3O$-based MOFs in most applications. We have used DFT to study the CO and NO adsorption on metal nodes of $Fe_3O$-based MOFs, subject to thermal treatments of different efficacy. The calculations allowed us to characterize how the adsorption of small molecules on $Fe_3O$-based clusters evolves with the coverage and how the desorption of chemisorbed species (water molecules and counteranions) affects the interaction of the clusters with adsorbates. We compared the simulated IR bands of CO and NO with experimental spectra reported in the literature. The calculations reproduce the changes observed in the spectra. NO showed a larger sensitivity to the presence of adsorbed species than CO at all coverages, and it is then a more suitable molecular probe for quick quality control checks. On the basis of the calculations, we propose to reassign some of the bands previously inaccurately assigned because of the absence of reference data on systems with a structure close to the $Fe_3O$ structure. Several experimental bands were formerly associated with a large concentration of defects. These bands are here reassigned by considering only crystallographic sites. These findings help in changing the common belief that MILs are highly defective materials and are useful for a more precise assignment of the CO and NO bands in iron-based MOFs, confirming the importance of the synergy between theory and experiments.

The calculated enthalpy of adsorption for both CO and NO was also assessed using the experimental data and compared with the enthalpy of adsorption of water, present often in the different applications of $Fe_3O$-based MOFs, as a contaminant or as a solvent. The importance of the interaction of CO and NO with $Fe_3O$-based MOFs plays a role in important MOF applications like drug delivery[1,4,11,12,21−23] and gas mixture purification.[19,4,20] Future studies should be aimed at enlarging the set of theoretical IR spectra of adsorbates on $Fe_3O$-based MOFs, including common probe molecules such as pyridine.

## ■ ASSOCIATED CONTENT

### Supporting Information

The Supporting Information is available free of charge at https://pubs.acs.org/doi/10.1021/acs.inorgchem.1c01044.

Additional energetic and electronic parameters for all of the clusters and Cartesian coordinates of all of the optimized structures (PDF)

## ■ AUTHOR INFORMATION


### Corresponding Authors

**Jenny G. Vitillo** − *Department of Science and High Technology and INSTM, University of Insubria, 22100 Como, Italy; Department of Chemistry, Chemical Theory Center, and Supercomputing Institute, University of Minnesota, Minneapolis, Minnesota 55455-0431, United States;* orcid.org/0000-0002-6213-2039; Email: jg.vitillo@gmail.com

**Laura Gagliardi** − *Department of Chemistry, Pritzker School of Molecular Engineering, James Franck Institute, University of Chicago, Chicago, Illinois 60637, United States;* orcid.org/0000-0001-5227-1396; Email: lgagliardi@uchicago.edu

Complete contact information is available at: https://pubs.acs.org/10.1021/acs.inorgchem.1c01044


### Author Contributions

The manuscript was written through contributions of all authors. All authors have given approval to the final version of the manuscript.

### Notes

The authors declare no competing financial interest.

## ■ ACKNOWLEDGMENTS

This work was supported by the Inorganometallic Catalyst Design Center, an EFRC funded by the Department of Energy, Office of Basic Energy Sciences (DE-SC0012702). The authors acknowledge the Minnesota Supercomputing Institute at the University of Minnesota for providing computational resources. Aditya Bhan, Matthew C. Simons, and Connie C. Lu are acknowledged for useful discussions.

## ■ REFERENCES


(1) Horcajada, P.; Serre, C.; Vallet-Regí, M.; Sebban, M.; Taulelle, F.; Férey, G. Metal-Organic Frameworks as Efficient Materials for Drug Delivery. *Angew. Chem., Int. Ed.* **2006**, *45* (36), 5974−5978.

(2) Horcajada, P.; Surble, S.; Serre, C.; Hong, D.-Y.; Seo, Y.-K.; Chang, J.-S.; Greneche, J.-M.; Margiolaki, I.; Ferey, G. Synthesis and catalytic properties of MIL-100(Fe), an iron(iii) carboxylate with large pores. *Chem. Commun.* **2007**, No. 27, 2820−2822.

(3) Yoon, J. W.; Chang, H.; Lee, S.-J.; Hwang, Y. K.; Hong, D.-Y.; Lee, S.-K.; Lee, J. S.; Jang, S.; Yoon, T.-U.; Kwac, K.; Jung, Y.; Pillai, R. S.; Faucher, F.; Vimont, A.; Daturi, M.; Ferey, G.; Serre, C.; Maurin, G.; Bae, Y.-S.; Chang, J.-S. Selective nitrogen capture by porous hybrid materials containing accessible transition metal ion sites. *Nat. Mater.* **2017**, *16* (5), 526−531.

(4) Yoon, J. W.; Seo, Y.-K.; Hwang, Y. K.; Chang, J.-S.; Leclerc, H.; Wuttke, S.; Bazin, P.; Vimont, A.; Daturi, M.; Bloch, E.; Llewellyn, P. L.; Serre, C.; Horcajada, P.; Grenèche, J.-M.; Rodrigues, A. E.; Férey, G. Controlled Reducibility of a Metal-Organic Framework with Coordinatively Unsaturated Sites for Preferential Gas Sorption. *Angew. Chem., Int. Ed.* **2010**, *49* (34), 5949−5952.

(5) Leclerc, H.; Vimont, A.; Lavalley, J.-C.; Daturi, M.; Wiersum, A. D.; Llwellyn, P. L.; Horcajada, P.; Ferey, G.; Serre, C. Infrared study of the influence of reducible iron(iii) metal sites on the adsorption of CO,

CO2, propane, propene and propyne in the mesoporous metal-organic framework MIL-100. *Phys. Chem. Chem. Phys.* **2011**, *13* (24), 11748−11756.
(6) Jeremias, F.; Khutia, A.; Henninger, S. K.; Janiak, C. MIL-100(Al,Fe) as water adsorbents for heat transformation purposes-a promising application. *J. Mater. Chem.* **2012**, *22* (20), 10148−10151.
(7) Al-Dadah, R.; Mahmoud, S.; Elsayed, E.; Youssef, P.; Al-Mousawi, F. Metal-organic framework materials for adsorption heat pumps. *Energy* **2020**, *190*, 116356.
(8) Vitillo, J. G.; Bhan, A.; Cramer, C. J.; Lu, C. C.; Gagliardi, L. Quantum Chemical Characterization of Structural Single Fe(II) Sites in MIL-Type Metal-Organic Frameworks for the Oxidation of Methane to Methanol and Ethane to Ethanol. *ACS Catal.* **2019**, *9* (4), 2870−2879.
(9) Simons, M. C.; Vitillo, J. G.; Babucci, M.; Hoffman, A. S.; Boubnov, A.; Beauvais, M. L.; Chen, Z.; Cramer, C. J.; Chapman, K. W.; Bare, S. R.; Gates, B. C.; Lu, C. C.; Gagliardi, L.; Bhan, A. Structure, Dynamics, and Reactivity for Light Alkane Oxidation of Fe(II) Sites Situated in the Nodes of a Metal-Organic Framework. *J. Am. Chem. Soc.* **2019**, *141* (45), 18142−18151.
(10) Guesh, K.; Caiuby, C. A. D.; Mayoral, Á.; Díaz-García, M.; Díaz, I.; Sanchez-Sanchez, M. Sustainable Preparation of MIL-100(Fe) and Its Photocatalytic Behavior in the Degradation of Methyl Orange in Water. *Cryst. Growth Des.* **2017**, *17* (4), 1806−1813.
(11) Agostoni, V.; Chalati, T.; Horcajada, P.; Willaime, H.; Anand, R.; Semiramoth, N.; Baati, T.; Hall, S.; Maurin, G.; Chacun, H.; Bouchemal, K.; Martineau, C.; Taulelle, F.; Couvreur, P.; Rogez-Kreuz, C.; Clayette, P.; Monti, S.; Serre, C.; Gref, R. Towards an Improved anti-HIV Activity of NRTI via Metal-Organic Frameworks Nanoparticles. *Adv. Healthcare Mater.* **2013**, *2* (12), 1630−1637.
(12) Marquez, A. G.; Hidalgo, T.; Lana, H.; Cunha, D.; Blanco-Prieto, M. J.; Alvarez-Lorenzo, C.; Boissiere, C.; Sanchez, C.; Serre, C.; Horcajada, P. Biocompatible polymer-metal-organic framework composite patches for cutaneous administration of cosmetic molecules. *J. Mater. Chem. B* **2016**, *4* (43), 7031−7040.
(13) Santiago-Portillo, A.; Navalón, S.; Cirujano, F. G.; Xamena, F. X. L. i.; Alvaro, M.; Garcia, H. MIL-101 as Reusable Solid Catalyst for Autoxidation of Benzylic Hydrocarbons in the Absence of Additional Oxidizing Reagents. *ACS Catal.* **2015**, *5* (6), 3216−3224 and references cited therein.
(14) Wuttke, S.; Bazin, P.; Vimont, A.; Serre, C.; Seo, Y.-K.; Hwang, Y. K.; Chang, J.-S.; Férey, G.; Daturi, M. Discovering the Active Sites for C3 Separation in MIL-100(Fe) by Using Operando IR Spectroscopy. *Chem. - Eur. J.* **2012**, *18* (38), 11959−11967.
(15) Cabello, C. P.; Berlier, G.; Magnacca, G.; Rumori, P.; Palomino, G. T. Enhanced $CO_2$ adsorption capacity of amine-functionalized MIL-100(Cr) metal-organic frameworks. *CrystEngComm* **2015**, *17* (2), 430−437.
(16) Zecchina, A.; Rivallan, M.; Berlier, G.; Lamberti, C.; Ricchiardi, G. Structure and nuclearity of active sites in Fe-zeolites: comparison with iron sites in enzymes and homogeneous catalysts. *Phys. Chem. Chem. Phys.* **2007**, *9* (27), 3483−3499.
(17) Hadjiivanov, K. I.; Panayotov, D. A.; Mihaylov, M. Y.; Ivanova, E. Z.; Chakarova, K. K.; Andonova, S. M.; Drenchev, N. L. Power of Infrared and Raman Spectroscopies to Characterize Metal-Organic Frameworks and Investigate Their Interaction with Guest Molecules. *Chem. Rev.* **2021**, *121* (3), 1286−1424.
(18) Haouas, M.; Volkringer, C.; Loiseau, T.; Férey, G.; Taulelle, F. Monitoring the Activation Process of the Giant Pore MIL-100(Al) by Solid State NMR. *J. Phys. Chem. C* **2011**, *115* (36), 17934−17944.
(19) Bonino, F.; Chavan, S.; Vitillo, J. G.; Groppo, E.; Agostini, G.; Lamberti, C.; Dietzel, P. D. C.; Prestipino, C.; Bordiga, S. Local structure of CPO-27-Ni metallorganic framework upon dehydration and coordination of NO. *Chem. Mater.* **2008**, *20* (15), 4957−4968.
(20) Chavan, S.; Vitillo, J. G.; Groppo, E.; Bonino, F.; Lamberti, C.; Dietzel, P. D. C.; Bordiga, S. CO Adsorption on CPO-27-Ni Coordination Polymer: Spectroscopic Features and Interaction Energy. *J. Phys. Chem. C* **2009**, *113* (8), 3292−3299.
(21) Tsai, M.-L.; Tsou, C.-C.; Liaw, W.-F. Dinitrosyl Iron Complexes (DNICs): From Biomimetic Synthesis and Spectroscopic Characterization toward Unveiling the Biological and Catalytic Roles of DNICs. *Acc. Chem. Res.* **2015**, *48* (4), 1184−1193.
(22) Carné-Sánchez, A.; Carmona, F. J.; Kim, C.; Furukawa, S. Porous materials as carriers of gasotransmitters towards gas biology and therapeutic applications. *Chem. Commun.* **2020**, *56* (68), 9750−9766.
(23) McKinlay, A. C.; Xiao, B.; Wragg, D. S.; Wheatley, P. S.; Megson, I. L.; Morris, R. E. Exceptional Behavior over the Whole Adsorption-Storage-Delivery Cycle for NO in Porous Metal Organic Frameworks. *J. Am. Chem. Soc.* **2008**, *130* (31), 10440−10444.
(24) Eubank, J. F.; Wheatley, P. S.; Lebars, G.; McKinlay, A. C.; Leclerc, H.; Horcajada, P.; Daturi, M.; Vimont, A.; Morris, R. E.; Serre, C. Porous, rigid metal(III)-carboxylate metal-organic frameworks for the delivery of nitric oxide. *APL Mater.* **2014**, *2* (12), 124112.
(25) Zhao, Y.; Truhlar, D. G. The M06 suite of density functionals for main group thermochemistry, thermochemical kinetics, noncovalent interactions, excited states, and transition elements: two new functionals and systematic testing of four M06-class functionals and 12 other functionals. *Theor. Chem. Acc.* **2008**, *120* (1), 215−241.
(26) Weigend, F. Accurate Coulomb-fitting basis sets for H to Rn. *Phys. Chem. Chem. Phys.* **2006**, *8* (9), 1057−1065.
(27) Weigend, F.; Ahlrichs, R. Balanced basis sets of split valence, triple zeta valence and quadruple zeta valence quality for H to Rn: Design and assessment of accuracy. *Phys. Chem. Chem. Phys.* **2005**, *7* (18), 3297−3305.
(28) Frisch, M. J.; Trucks, G. W.; Schlegel, H. B.; Scuseria, G. E.; Robb, M. A.; Cheeseman, J. R.; Scalmani, G.; Barone, V.; Petersson, G. A.; Nakatsuji, H.; Li, X.; Caricato, M.; Marenich, A. V.; Bloino, J.; Janesko, B. G.; Gomperts, R.; Mennucci, B.; Hratchian, H. P.; Ortiz, J. V.; Izmaylov, A. F.; Sonnenberg, J. L.; Williams Ding, F.; Lipparini, F.; Egidi, F.; Goings, J.; Peng, B.; Petrone, A.; Henderson, T.; Ranasinghe, D.; Zakrzewski, V. G.; Gao, J.; Rega, N.; Zheng, G.; Liang, W.; Hada, M.; Ehara, M.; Toyota, K.; Fukuda, R.; Hasegawa, J.; Ishida, M.; Nakajima, T.; Honda, Y.; Kitao, O.; Nakai, H.; Vreven, T.; Throssell, K.; Montgomery, J. A., Jr.; Peralta, J. E.; Ogliaro, F.; Bearpark, M. J.; Heyd, J. J.; Brothers, E. N.; Kudin, K. N.; Staroverov, V. N.; Keith, T. A.; Kobayashi, R.; Normand, J.; Raghavachari, K.; Rendell, A. P.; Burant, J. C.; Iyengar, S. S.; Tomasi, J.; Cossi, M.; Millam, J. M.; Klene, M.; Adamo, C.; Cammi, R.; Ochterski, J. W.; Martin, R. L.; Morokuma, K.; Farkas, O.; Foresman, J. B.; Fox, D. J. *Gaussian 16*, revision B.01; Gaussian Inc.: Wallingford, CT, 2016.
(29) Verma, P.; Vogiatzis, K. D.; Planas, N.; Borycz, J.; Xiao, D. J.; Long, J. R.; Gagliardi, L.; Truhlar, D. G. Mechanism of Oxidation of Ethane to Ethanol at Iron(IV)-Oxo Sites in Magnesium-Diluted Fe2(dobdc). *J. Am. Chem. Soc.* **2015**, *137* (17), 5770−5781.
(30) Mavrandonakis, A.; Vogiatzis, K. D.; Boese, A. D.; Fink, K.; Heine, T.; Klopper, W. Ab Initio Study of the Adsorption of Small Molecules on Metal-Organic Frameworks with Oxo-centered Trimetallic Building Units: The Role of the Undercoordinated Metal Ion. *Inorg. Chem.* **2015**, *54* (17), 8251−8263.
(31) Vitillo, J. G.; Lu, C. C.; Cramer, C. J.; Bhan, A.; Gagliardi, L. Influence of First and Second Coordination Environment on Structural Fe(II) Sites in MIL-101 for C-H Bond Activation in Methane. *ACS Catal.* **2021**, *11* (2), 579−589.
(32) Boys, S. F.; Bernardi, F. The calculation of small molecular interactions by the differences of separate total energies. Some procedures with reduced errors. *Mol. Phys.* **1970**, *19*, 553−566.
(33) De Moor, B. A.; Reyniers, M.-F.; Marin, G. B. Physisorption and chemisorption of alkanes and alkenes in H-FAU: a combined ab initio-statistical thermodynamics study. *Phys. Chem. Chem. Phys.* **2009**, *11* (16), 2939−2958.
(34) Grimme, S. Supramolecular Binding Thermodynamics by Dispersion-Corrected Density Functional Theory. *Chem. - Eur. J.* **2012**, *18* (32), 9955−9964.
(35) Ribeiro, R. F.; Marenich, A. V.; Cramer, C. J.; Truhlar, D. G. Use of Solution-Phase Vibrational Frequencies in Continuum Models for the Free Energy of Solvation. *J. Phys. Chem. B* **2011**, *115* (49), 14556−14562.
(36) Zhao, Y.; Truhlar, D. G. Computational characterization and modeling of buckyball tweezers: density functional study of concave-


https://doi.org/10.1021/acs.inorgchem.1c01044
*Inorg. Chem.* 2021, 60, 11813−11824

convex 3···· interactions. *Phys. Chem. Chem. Phys.* **2008**, *10* (19), 2813−2818.
(37) John, M.; Alexopoulos, K.; Reyniers, M.-F.; Marin, G. B. Mechanistic insights into the formation of butene isomers from 1-butanol in H-ZSM-5: DFT based microkinetic modelling. *Catal. Sci. Technol.* **2017**, *7* (5), 1055−1072.
(38) Isley, W., III. https://github.com/william-isley-3rd/Comp-Chem-Tools (accessed 2018-06-12).
(39) Marenich, A. V.; Jerome, S. V.; Cramer, C. J.; Truhlar, D. G. Charge Model 5: An Extension of Hirshfeld Population Analysis for the Accurate Description of Molecular Interactions in Gaseous and Condensed Phases. *J. Chem. Theory Comput.* **2012**, *8* (2), 527−541.
(40) Ritchie, J. P.; Bachrach, S. M. Some methods and applications of electron density distribution analysis. *J. Comput. Chem.* **1987**, *8* (4), 499−509.
(41) Gaggioli, C. A.; Stoneburner, S. J.; Cramer, C. J.; Gagliardi, L. Beyond Density Functional Theory: The Multiconfigurational Approach To Model Heterogeneous Catalysis. *ACS Catal.* **2019**, *9* (9), 8481−8502.
(42) Gani, T. Z. H.; Kulik, H. J. Understanding and Breaking Scaling Relations in Single-Site Catalysis: Methane to Methanol Conversion by FeIV-O. *ACS Catal.* **2018**, *8* (2), 975−986.
(43) Rosen, A. S.; Notestein, J. M.; Snurr, R. Q. Structure-Activity Relationships That Identify Metal-Organic Framework Catalysts for Methane Activation. *ACS Catal.* **2019**, *9* (4), 3576−3587.
(44) Valenzano, L.; Civalleri, B.; Chavan, S.; Palomino, G. T.; Areán, C. O.; Bordiga, S. Computational and Experimental Studies on the Adsorption of CO, $N_2$, and $CO_2$ on Mg-MOF-74. *J. Phys. Chem. C* **2010**, *114* (25), 11185−11191.
(45) Vitillo, J. G.; Ricchiardi, G. Effect of Pore Size, Solvation, and Defectivity on the Perturbation of Adsorbates in MOFs: The Paradigmatic $Mg_2$(dobpdc) Case Study. *J. Phys. Chem. C* **2017**, *121* (41), 22762−22772.
(46) Bonino, F.; Lamberti, C.; Chavan, S.; Vitillo, J. G.; Bordiga, S. Characterization of MOFs. 1. Combined Vibrational and Electronic Spectroscopies. In *Metal Organic Frameworks as Heterogeneous Catalysts*; Llabrés i Xamena, F. X., Gascon, J., Eds.; The Royal Society of Chemistry, 2013; pp 76−142.
(47) Jensen, S.; Tan, K.; Feng, L.; Li, J.; Zhou, H.-C.; Thonhauser, T. Porous Ti-MOF-74 Framework as a Strong-Binding Nitric Oxide Scavenger. *J. Am. Chem. Soc.* **2020**, *142* (39), 16562−16568.
(48) Dhakshinamoorthy, A.; Alvaro, M.; Horcajada, P.; Gibson, E.; Vishnuvarthan, M.; Vimont, A.; Grenèche, J.-M.; Serre, C.; Daturi, M.; Garcia, H. Comparison of Porous Iron Trimesates Basolite F300 and MIL-100(Fe) As Heterogeneous Catalysts for Lewis Acid and Oxidation Reactions: Roles of Structural Defects and Stability. *ACS Catal.* **2012**, *2* (10), 2060−2065.
(49) McKinlay, A. C.; Eubank, J. F.; Wuttke, S.; Xiao, B.; Wheatley, P. S.; Bazin, P.; Lavalley, J. C.; Daturi, M.; Vimont, A.; De Weireld, G.; Horcajada, P.; Serre, C.; Morris, R. E. Nitric Oxide Adsorption and Delivery in Flexible MIL-88(Fe) Metal-Organic Frameworks. *Chem. Mater.* **2013**, *25* (9), 1592−1599.
(50) Ford, P. C.; Lorkovic, I. M. Mechanistic Aspects of the Reactions of Nitric Oxide with Transition-Metal Complexes. *Chem. Rev.* **2002**, *102* (4), 993−1018.


https://doi.org/10.1021/acs.inorgchem.1c01044
*Inorg. Chem.* 2021, 60, 11813−11824